Plasmon-Resonant Vibrational Sum Frequency Generation of Electrochemical Interfaces: Direct Observation of Carbon Dioxide Electroreduction on Gold

Spencer Wallentine, Savini Bandaranayake, Somnath Biswas, and L. Robert Baker* Department of Chemistry and Biochemistry, The Ohio State University, Columbus, OH 43210 Received August 20, 2020; E-mail: baker.2364@osu.edu

Abstract:

Here we present a plasmon-resonant vibrational sum frequency generation spectroscopy for use in electrochemical measurements. Using surface plasmon resonance we couple light through a CaF₂ prism to Au films of > 50 nm in order to reach the buried Au/electrolyte interface. The approach enables us to use bulk electrolyte, and high current densities (> 1mA/cm²), and therefore is suitable to probe active intermediates under relevant electrochemical reaction conditions. Fresnel factor modeling of the plasmon resonance for a three layer system (CaF₂/Au/electrolyte) shows good agreement with experimental data. Off-angle momentum-matching to the surface plasmon resonance allows us to measure functional groups(-CH, -CD, -CN, -NO₂) across a wide range of infrared frequencies by simply scanning the infrared wavelength without any angular realignment . Additionally we report a detection limit < 1%of a monolayer for the Au/electrolyte interface. Using this method we observe an active intermediate during CO2 reduction on Au at catalytic currents. Consequently, we believe that this method will provide mechanistic understanding of electrochemical reactions.

1. Introduction

Due to the low detection limits and inherent surface sensitivity of Vibrational Sum Frequency Generation (VSFG) spectroscopy, it has become a useful tool for the study of electrochemical interfaces. $^{1-6}$ VSFG is a second order nonlinear process that occurs between two fields of different frequencies, often a fixed visible field and a broadband or tunable infrared field. $^{7-9}$ As a second order process, VSFG inherently ignores contributions from centrosymmetric media and is therefore interface specific in the dipole approximation

Use of this technique for electrochemical measurements remains experimentally challenging due to the difficulty of transmitting an infrared beam to an electrode/electrolyte interface under working electrochemical conditions. This is because most electrodes are opaque to infrared light, and many electrolytes, including water, also strongly absorb a large portion of the mid-infrared spectrum. 2,10,11 Although many conductors show weak transmission of IR light, notable exceptions exist. This includes ITO, which is transmissive in certain regions of the IR spectrum and can provide a spectral window to the electrode/electrolyte interface. 12 To address this challenge, two experimental geometries have previously been employed for VSFG studies of electrochemical systems. However, as discussed below, each of these possess experimental drawbacks, which have limited their wide spread application for spectroelectrochemistry.

The first method employs a front side geometry, shown in Figure 1a, where the visible and infrared beams approach the

interface from the electrolyte side. $^{2,13-16}$ The benefit of this approach is that it enables the use of a bulk electrode that can be well-characterized and sustain a high current density. However, the disadvantage of this approach is that both visible and infrared beams must pass through the electrolyte, which severely attenuates the infrared intensity. For this reason, when working in this geometry, the electrode is pressed close against an optical element such as a prism with only an ultrathin (< 50 $\mu \rm m$) film of electrolyte sandwiched against the electrode surface. $^{2-4,14,15}$ While this enables transmission of infrared light to the electrode/electrolyte interface, it results in severe mass transport limitations when attempting to probe faradaic processes, which can introduce experimental artifacts resulting from pH gradients and diffusion controlled kinetics.

The second method is for the visible and infrared beams to approach the interface through the electrode as shown in Figure 1b. 10,17-19 While this technique avoids the need for ultrathin electrolyte layers, it requires the use of a transparent electrode. Since conductive materials are by nature strong absorbers (or reflectors) of infrared light, this geometry presents major challenges by severely limiting selection of the electrode material. A common approach in this area has been to employ ultrathin metal electrodes (i.e. ≤ 10 nm), which are semitransparent yet moderately conductive. 1,20 However, the signal-to-noise in these geometries is typically poor owing to the unfavorable Fresnel factor. 10,18,20 Additionally, films with average thickness less than 10 nm are often unstable and cannot sustain the current densities required for electrocatalysis due to resistive heating of the ultrathin film.

To improve signal-to-noise in this backside approach, a variation to the second method has been reported where a thicker electrode is employed to produce a surface plasmon resonance (SPR) enhancement of the Fresnel factor. ^{1,19,21–23} This has been shown to significantly improve signal-to-noise and has promise for electrocatalysis since the thicker metal film can also sustain higher current densities necessary to study electrocatalytic processes.

SPR coupling is realized through phase-matching the incident 800 nm laser field with the momentum vector of the

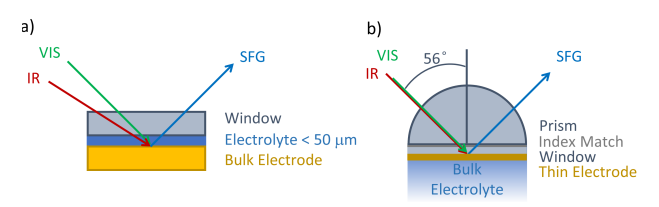


Figure 1. a) Frontside or thin electrolyte geometry. b) Backside or co-propagating Kretschmann geometry employed in experiments in this work.

surface plasmon. However, this is only one type of phase matching that occurs during a plasmon-enhanced SFG measurement. To clarify, we note that there are three types of phase-matching referred to in this paper: 1) Phase-matching between the visible and IR laser beams to generate VSFG signal. This phase matching is required for all VSFG spectroscopy even without SPR enhancement. While the plasma response of the metal substrate may assist in this process, the only required phase-matching occurs between the visible and IR wavevectors. 2) Phase-matching between the incident IR beam and an SPR in the metal, which would lead to an enhancement of the IR field. 3) Phase-matching between the incident 800 nm field and an SPR in the metal, which would lead to an enhancement of the 800 nm field. This third type of phase-matching where an SPR enhances the 800 nm electric field at the Au electrode/electrolyte interface is the main focus of this paper, and provides an advantage over IR-SPR coupling as the coupling angle does not change with IR wavelength as discussed below.

Plasmon resonant VSFG was first applied to electrochemical systems by Shen and co-workers, where coupling to an SPR occurred through phase-matching of the infrared field, and resulted in enhanced detection of dodecanethiol on Au during electrochemical cycling. 1 The phase-matching angle required to couple light into an SPR is narrow and is strongly dependent on the wavelength of light as well as the dielectric functions of the substrate, the metal layer, and the backside medium. ²⁴ In an electrochemical VSFG experiment these layers correspond to the prism, the electrode, and the electrolyte. Accordingly, working at an infrared SPR in practice requires tedious realignment of the laser fields for each region of the infrared spectrum to be measured as well as for different electrolytes. For example, the SPR enhancement measured for the Au/D₂O interface was limited to a single narrow frequency range and signal was lost when the backside medium was switched from D₂O to H₂O without angular realignment. 1

Here we present an off-angle momentum-matched, plasmon enhanced VSFG technique for electrochemical applications. Relaxation of the angle requirement for SPR is simply achieved by electron beam deposition of Au directly onto a ${\rm CaF_2}$ window in the absence of an adhesion layer resulting in a nanostructured ${\rm Au/CaF_2}$ buried interface. A number of possible mechanism are discussed, which can couple the 800 nm field to the SPR wavevector, leading to an enhanced VSFG signal. The net result of off-angle SPR momentum matching is the ability to probe the buried electrode/electrolyte interface with high sensitivity across the entire infrared spectral range during an electrochemical reaction without any realignment. We show that detection limits less than 1% of a monolayer are easily achievable at the ${\rm Au/electrolyte}$ interface, even with short integration times.

Using this technique, we demonstrate the ability to measure in-situ generated CO with high signal-to-noise during CO_2 reduction on Au. Directly observing active surface intermediates represents a significant challenge in electrocatalysis. This is especially true for CO_2 electroreduction on Au electrodes because weak CO adsorption leads to very low surface coverage during steady state turnover. 25,26 Consequently, this method answers a long-standing challenge in Au electrocatalysis, and promises to inform a variety of processes occurring at active electrochemical interfaces.

2. Methods

Materials and Sample Preparation

Perfluorodecane was purchased from Floryx Laboratories, d-25-1-dodecanethiol was purchased from CDN isotopes, and 4-mercaptobenzonitrile was purchased from Enamine. All other chemicals were purchased from Sigma Aldrich. Chemicals were used as purchased without further purification. Au electrodes were prepared by electron beam evaporation on infrared grade CaF₂ windows (Eksma) using a Kurt J. Lesker Lab-18 deposition system. Film thickness was monitored during deposition by quartz crystal microbalance, and resulting thicknesses were calibrated using atomic force microscopy. Self-assembled monolayers (SAMs) were prepared on the Au electrodes by first cleaning the Au in either 2 mTorr of air plasma (Harrick Plasma PDC-001) on medium power for 30 seconds or by dropping 40 vol% nitric acid on the Au surface for 20 seconds and immediately washing with milli-Q water. Both methods for cleaning yielded good results as determined by VSFG and electrochemical cyclic voltametry measurements. The cleaned Au films were then immersed in 1-dodecanethiol (2 mM), d25-dodecanethiol (2 mM), 4-nitrothiophenol (2 mM), thiophenol (4 mM), or 4-mercaptobenzonitrile (4 mM) in ethanol and kept in solution overnight. Upon removal from solution, these various SAMs were washed with ethanol and dried under nitrogen prior to use.

Electrochemical Measurements

All electrochemical measurements were made using a Biologic SP-50 potentiostat on 27 nm Au films. Electrolyte solutions of sodium bicarbonate (0.1 M) were prepared using milli-Q water and were purged with CO₂ at 300 sccm until the solution pH was 6.8. All potentials were recorded vs Ag/AgCl (3M NaCl) using a platinum mesh counter electrode. Prior to making measurements, the electrode was cycled from $0.3~\mathrm{V}$ to $-1.1~\mathrm{V}$ to ensure a clean electrochemical surface. A nafion proton exchange membrane separated the working and counter electrodes. Spectra showing CO were collected using a step potential sequence with integration for 60 seconds. Measurements were made after the electrode equilibrated to the applied potential. The cyclic voltammogram was collected with a scan rate of 50 mV/s. Current density was calculated using the geometric area of the electrode. Au electrodes are stable between 0.3 V and -1.1 V vs Ag/AgCl even in the absence of a Cr adhesion layer. However, we cannot comment on electrode stability at potentials more positive than 0.3 V. At potentials more negative than -1.1 V the gold film has a tendency to delaminate over time, and this becomes increasingly probable at more negative potentials. Despite this, we find that it is possible to collect spectra with integration times up to several minutes at potential as negative as -1.7 V.

Sum Frequency Generation Spectroscopy

The VSFG system has been described previously. ²⁷ However, we provide additional details pertaining to the electrochemical VSFG measurements reported here for the first time. Spectra were measured in a custom spectroelectrochemical cell (See supporting information section 1). For VSFG measurements, the 800 nm pulse energy was \sim 10 μ J and the infrared energy was \sim 5 μ J. To probe various polarization combinations, the infrared polarization was controlled with a half waveplate and the 800 nm and the VSFG signal beams were each controlled using a half waveplate

and polarizer. Other polarization combinations are shown in the supporting information section 2. Unless otherwise noted spectra were taken in PPP (P polarized VSFG, 800 nm, and infrared) polarization. Suppression of non-resonant signal was achieved by introducing a temporal delay to the time-asymmetric 800 nm pulse relative to the infrared pulse 9 corresponding to 530 fs in the CH region and 670 fs in the CN and CO regions. Unless otherwise noted, spectra were integrated for 60 seconds. A purge box encloses the infrared beam path and sample chamber that can be flushed with dry $\rm N_2$ to remove spectral absorption from ambient water and $\rm CO_2$.

X-ray Photoelectron Spectroscopy

X-ray Photoelectron Spectroscopy (XPS) analysis was performed to quantify the relative surface coverage of mixed SAMs consisting of 4-mercaptobenzonitrile and thiophenol using a Kratos Axis Ultra x-ray photo-electron spectrometer (monochromatic Al K α X-ray source, $E_{photon} = 1486.6$ eV, pass energy 80 eV). Spectra were collected for SAMs prepared from mixed solutions of 4-mercaptobenzonitrile and thiophenol in ethanol (4mM total concentration) consisting of 10, 20, 40, 60, 80, and 100 percent 4-mercaptobenzonitrile. As described in the main manuscript below, this XPS data was fit to a competitive isotherm model to extract the relative binding constants for 4-mercaptobenzonitrile and thiophenol on Au. This information was then used to prepare SAMs with a precisely known surface coverage of 4mercaptobenzonitrile for quantitatively determining VSFG detection limits.

3. Results and Discussion

The primary disadvantage of using an SPR enhancement is the strict phase-matching required to produce a plasmon resonance. In order for light to couple into an SPR mode, the component of the wavevector parallel to the interface must match the wavevector of the plasmon resonance as shown in Equation $1.^{28}$

$$k_{SPR} = k_x = \frac{2\pi n_1 sin(\theta)}{\lambda} \tag{1}$$

Here k_{SPR} is the wavevector of the SPR mode, k_x is the component of the laser wavevector parallel to the metal/dielectric interface in p-polarization, n_1 is the refractive index of the prism, λ is the wavelength of the incident light, and θ is the incident angle of the light relative to surface normal. This condition can be satisfied for a few materials in the visible spectrum and near infrared (Au, Ag, Cu, and Al). While this momentum matching is most commonly achieved by prism coupling at a precise incidence angle, a number of mechanisms exist that can allow SPR excitation at a range of incidence angles, and these are briefly described below.

Prism coupling is the typical method for SPR excitation. This is accomplished by angle tuning of the incident field in a high index medium until the k_x vector of the incident field matches the SPR wavevector, k_{SPR} . In prism coupling the singular resonance angle is extremely sensitive to changes in the refractive index of the backside medium. Consequently, it is commonly employed analytically to detect binding of a substrate to a metal surface. ²⁹ If this were the primary mechanism for SPR excitation in the present study, then signal enhancement would be a sensitive function of incidence

angle, refractive index of the electrolyte, and IR frequency, which is not the case as shown below.

Grating coupling uses the diffraction orders of a grating (positive or negative) to borrow the momenta necessary to satisfy the momentum matching condition as given by Equation 2:

$$k_{SPR} = k_x \pm mg \tag{2}$$

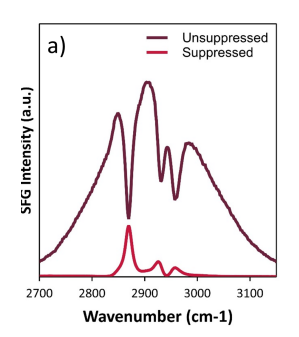
where m is the grating order, and g is the grating lattice constant, with $g=2\pi/a$, and a is the grating period. 28,30,31 Rough surface coupling represents a special case of grating coupling where a distribution of spatial features act as variable line spacings on a roughened surface such that the angle matching requirement appears to be relaxed. 28,30 In supporting information section 3, we analyze the spatial features of the electrodes employed here and show that these can support SPR coupling through the grating effect.

Localized surface plasmon resonances (LSPR) also exist on nanostructured metals and have been shown to excite propagating SRP modes by near field coupling. ^{30,32,33} LSPR excitation does not require a specific angle due to the range of wavevectors contained in the spatially confined resonance, so this can allow coupling of light into a propagating SPR mode at a range of incidence angles. Here the intensity of the generated SPR is a function of the LSPR intensity and the LSPR-SPR coupling strength. As described in the supporting information section 3, both LSPR excitation as well as grating coupling on the roughened Au electrode can contribute to the VSFG signal enhancements demonstrated here, and additional work would be required to disentangle the specific contributions of each.

Figure 1b shows the co-propagating Kretschmann geometry used in our experiment, with the fields incident from the electrode side. In the Kretschmann geometry used here, the infrared and visible beams are incident at 56° in plane but are offset 5° out of plane. This out of plane offset does not contribute any polarization contamination to the measured VSFG signal as described in the supporting information section 4. The sum frequency beam is collected in reflection geometry. Exchangeable samples are made by evaporating Au electrodes of controlled thickness onto CaF₂ windows. Many electrodes can be prepared in parallel and are subsequently indexed-matched to a hemicylindrical CaF₂ prism using perfluorodecane as an infrared-transparent index match. This approach enables the reuse of the prism and facilitates high sample throughput on multiple disposable electrodes, which represents a significant advantage in time and cost compared to direct deposition of the electrode onto the hemicylindrical prism. Additional details on this approach are described in the supporting information (See supporting information section 1).

The experimentally measured spectra of a 53 nm Au film with a dodecanethiol self-assembled monolayer (SAM) are shown in Figure 2a. Unsuppressed spectra are obtained at maximum temporal overlap between 800 nm and broadband infrared pulses. Non-resonant suppressed spectra are obtained by delaying a time asymmetric 800 nm pulse relative to the infrared pulse, which selectively suppresses the non-resonant contribution of the signal due to its faster decoherence time compared with vibrational resonances. ^{34,35} The unsuppressed spectra can be fit to extract the resonant contribution as is typically done for VSFG spectra (see supporting information section 5). ^{8,19}

To investigate the effect of Au layer thickness on the res-



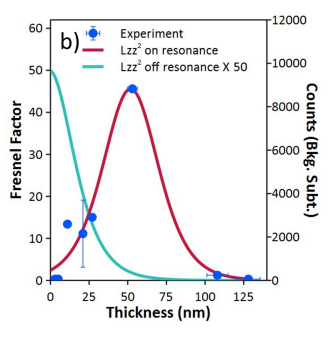


Figure 2. a) Unsuppressed and non-resonant suppressed VSFG signal from a self-assembled monolayer of 1-dodecanethiol on a 53 nm Au film b) Simulated three layer Fresnel factors on and off plasmon resonance for different film thicknesses plotted with the experimental data. The horizontal error is the standard deviation derived from the thickness calibration. The vertical error bar (shown only for the 27 nm data point) is a standard deviation derived from replicate samples.

onant VSFG signal, Figure 2b shows a simulation of the three layer transmission Fresnel factor at 800 nm for the CaF₂/Au/water interface as a function of Au layer thickness. 28,36 The details of these simulations and associated equations are given in the supporting information section 6. The data points in Figure 2b represent the experimentally measured resonant intensity of the 2,870 cm⁻¹ peak for dodecanethiol as a function of Au layer thickness. These data are compared to two thickness-dependent Fresnel factors: the on-resonance Fresnel factor is the Fresnel factor at the surface plasmon resonance angle of 73° for the CaF₂/Au/water interface. The off-resonance Fresnel factor is the Fresnel factor calculated at the experimental working angle of 56°, which is below the calculated plasmon resonance angle for this system. As shown, the on and offplasmon resonance Fresnel factors behave differently. The off-resonance Fresnel factor (multiplied by 50) predicts that the VSFG signal should decrease exponentially with thickness (i.e. less field transmits to the interface through thicker films), while the on-resonant Fresnel factor predicts a maximum electric field for Au film thickness of approximately 50 nm. As shown, the experimental VSFG intensity quantitatively follows the on-resonant Fresnel factor in Figure 2b showing a maximum enhancement for 53 nm Au films. This result may seem surprising because the simulated resonance angle for the CaF₂/Au/water interface is 73°, and our working angle is 56° relative to surface normal. However, this result can be explained by off-angle momentum matching of the SPR wavevector, which can occur either via grating coupling or LSPR coupling as described above. For additional details see also supporting information section 3.

Several additional experimental observations support this explanation for SPR enhancement of the VSFG signal based on relaxation of the strict angle matching requirement. First, Au films deposited on dielectric substrates such as CaF_2 grow in a non-continuous manner, forming a nanostructured CaF_2/Au interface, which would serve to relax the requirement for resonant momentum matching. 37,38 Scanning electron microscopy of the Au films grown on CaF_2 for these studies confirms this nanostructuring (see supporting information section 7). This nanostructuring may act as a plasmonic grating that can couple the incident 800 nm field into the SPR modes of the Au layer. When a Cr adhe-

sion layer is added to the CaF₂ window, the VSFG signal dramatically decreases, and resonant vibrations from the dodecanethiol SAM are not observed as shown in supporting information section 7. Section 3 of the supporting information provides a quantitative comparison based on image analysis of the Fourier components indicating that the Cr adhesion reduces SPR momentum matching via the grating mechanism. We also note that in addition to altering the spatial features of the Au electrode, Cr is known to damp the electric field produced by SPR excitation, which could also lead to the observation here. ^{39,40} Finally, we show that a $45~\mathrm{nm}$ Ni film, which is not plasmonic, shows less than 1%of the resonant signal coming from the dodecanethiol SAM compared to Au, even though these SAMs are well known to form on Ni as well as Au, 41 confirming the role of plasmon resonance on the observed signal (see supporting information section 7).

We note that propagating SPR modes are different from localized surface plasmon resonances or LSPR modes in that LSPR fields represent highly localized electric field enhancements, which often results in selective sampling of hot spots, while propagating SPR fields have a larger homogeneous spatial distribution, which results in more uniform sampling. Measuring the optical extinction of the Au films as a function of thickness shows that these samples lack the absorption feature typical of LSPR modes in Au (See supporting information section 8). ^{42–45} This observation may suggest that the SPR excitation occurs via the grating effect as opposed to LSPR coupling, although further work would be required to disentangle the specific contributions of these two effects.

The observed off-angle coupling has several important implications for practical experiments. First, no tedious alignment changes are required as the momentum vectors of the infrared and/or 800 nm fields change. That is, VSFG spectra can be obtained across the entire frequency range simply by scanning the infrared wavelength without any angular realignment. Figure 3 shows VSFG spectra from SAMs of a) 1-dodecanethiol, b) 4-mercaptobenzonitrile, c) d-25-1dodecanethiol, and d) 4-nitrothiophenol collected with water as the backside dielectric medium. The corresponding vibrational stretching frequencies of these compounds are in agreement with the literature values. 9,46-48 All spectra were collected in the same geometry and only required scanning the infrared wavelength. To further explain this, we calculate the three layer transmission Fresnel factor (L_{zz}^2) for the infrared beam across a wide range of frequencies (1250-3000 cm⁻¹), and this is shown in Figure S13 in the supporting information. We find that the Fresnel factor varies smoothly as a function of infrared frequency. This indicates that the SPR signal enhancement in this method comes primarily from the 800 nm field as opposed to the infrared field, giving rise to the ability to measure chemical functional groups spanning a wide frequency range. While the Fresnel factor modeling indicates that the primary enhancement comes from the 800 nm field, the possibility for plasmonic enhancement from the IR field should also not be completely ignored. In fact, IR field enhancements of similar electrodes are commonly observed in the related technique surface-enhanced IR absorption spectroscopy (SEIRAS), and 2D-IR, and it is likely that we are also benefiting from an additional IR enhancement here. $^{49-52}$

A second benefit of this method is that signal intensity is relatively insensitive to incident angles as shown in Figure 4a (see supporting information section 1). If these measure-

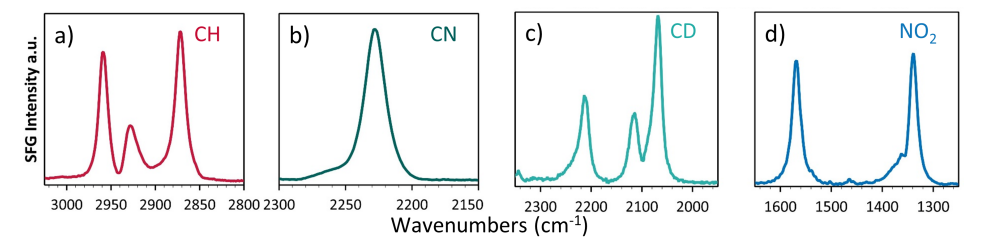


Figure 3. Unsuppressed VSFG spectra from self assembled monolayers for a) 1-dodecanethiol, b) 4-mercaptobenzonitrile, c) d25-1-dodecanethiol, and d) 4-nitrothiophenol.

ments were made under typical plasmon resonance conditions, the signal should drop drastically as the angle is tuned off the sharp resonance. However, the VSFG intensity quantitatively scales as $\sec^2\theta_{SF}$ as predicted by Equation 3:

$$I_{SF} = \frac{8\pi^3 \omega^2 sec^2 \theta_{SF}}{\hbar c^3 \sqrt{\epsilon(\omega)\epsilon(\omega_1)\epsilon(\omega_2)}}$$

$$\times |e(\omega) \cdot \chi_s^{(2)} : e(\omega_1)e(\omega_2)|^2 I_1(\omega_1)I_2(\omega_2)$$
(3)

where θ_{SF} is the VSFG phase matching angle. ⁵³ Thus the plasmon enhancement of the VSFG signal is confirmed to be broad and flat in angular space. Third, VSFG signal is not affected by changes in the dielectric constant of the backside medium. Figure 4b shows VSFG spectra collected with air and water as the backside dielectric. Changing the backside medium does not significantly change the spectral profile or intensity. This is advantageous for electrochemical experiments where different electrochemical solvents, analytes, and electrolytes would change the refractive index causing the plasmon resonance to move under typical SPR conditions with strict momentum matching.

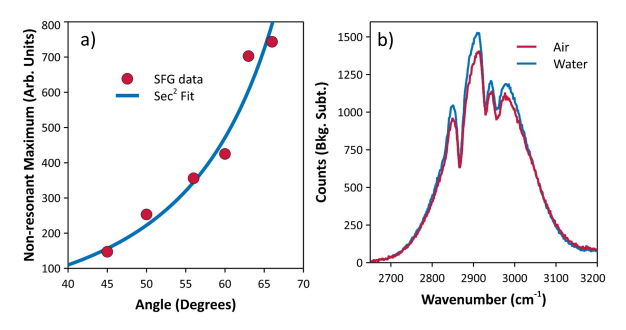


Figure 4. a) Observed \sec^2 scaling of the VSFG non-resonant signal as a function of the sum frequency angle. b) Unsuppressed VSFG spectra taken with air and water as the dielectric medium.

Equally important to the above outcomes is the detection limit. Figure 5a shows the CN stretch from 1% of a monolayer of 4-mercaptobenzonitrile collected in only 60 seconds integration time showing an excellent signal-to-noise ratio of approximately 40. In order to obtain this detection limit we prepared solutions with different concentrations of 4-mercaptobenzonitrile and thiophenol. Due to differences in the heats of adsorption, the solution concentrations are not exactly representative of surface concentrations. In order to quantify the relative surface concentrations of 4-mercaptobenzonitrile and thiophenol, we measured XPS at the N 1s and S 2p edges and plot the nitrogen/sulfur ratio as a function of the percent of 4-mercaptobenzonitrile in so-

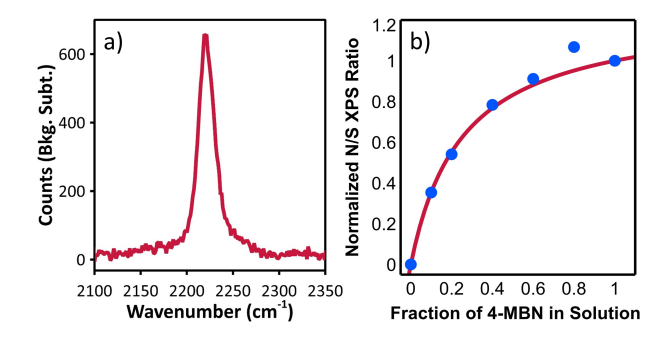


Figure 5. a) Non-resonant suppressed VSFG spectra from 1% of a monolayer of 4-mercaptobenzonitrile co-adsorbed with thiophenol b) Relative coverage obtained from the sulfur to nitrogen ratio from XPS as a function of 4-mercaptobenzonitrile in solution. The line is a fit to the data using a competitive binding isotherm and was used to determine the solution concentration needed to obtain 1% 4-mercaptobenzonitrile surface coverage.

lution (see supporting information section 9 for associated XPS spectra). Figure 5b shows the results of these measurements. The measured nitrogen/sulfur ratio was normalized to the 100% 4-mercaptobenzonitrile sample and fit using the competitive Langmuir isotherm in Equation 4:

$$\theta_a = \frac{K_{eq}^a[a]}{1 + K_{eq}^a[a] + K_{eq}^b[b]} \tag{4}$$

This result gives the relative equilibrium constants for 4-mercaptobenzonitrile (K^a_{eq}) and thiophenol (K^b_{eq}) , where $(K^a_{eq})/(K^b_{eq})$ is 4.9. Based on the relative equilibrium constants from this isotherm, we prepared Au electrodes functionalized with 4-mercaptobenzonitrile diluted in a layer of thiophenol, where nitrile groups were present at less than 1% concentration. The VSFG spectrum in Figure 5a represents the nitrile stretch from this sample measured with a 60 s integration. Detection limits on the order of a few percent of a monolayer are needed to observe catalytic reaction intermediates and other low occurrence surface species.

This is especially true for CO_2 electroreduction on Au electrodes because weak CO adsorption leads to very low surface coverage during steady state turnover. ^{54,55} Figure 6a shows a typical cyclic voltammogram collected in CO_2 purged 0.1 M sodium bicarbonate in the VSFG electrochemical cell. As shown, current densities in excess of 1 mA/cm² are readily obtained. Active purging of the bulk electrolyte with CO_2 at 300 mL/min provides a constant supply of fresh reactants to the electrode surface. The onset potential for

catalytic current occurs near -0.75 V vs Ag/AgCl.

Figure 6b shows that using off-angle momentum matched, plasmon-resonant VSFG, we can readily measure spectra of in-situ generated CO adsorbed on the Au electrode during reaction. These spectra were obtained during a potential step sequence. At the potentials noted, the potential was held fixed, and the electrode was allowed to polarize, then a 60 second VSFG spectrum was collected. The first spectrum shown in blue was obtained at the start of the cathodic scan at 0.2 V, which is below the onset potential for reaction. A small peak can be seen at 2,115 cm⁻¹, and this signal is from residual CO produced during preliminary CV cycling. As the bias is swept beyond the onset potential, the current density in the cell exceeds 1 mA/cm². This represents the faradaic current from a combination of CO₂ reduction and H₂ evolution. A second spectrum shown in black was measured at -1.5 V and shows surface bound CO during active electrocatalysis. Here a stronger signal is observed at 2,090 cm⁻¹, and this is consistent with CO adsorbed in the atop position on the Au electrode. 52,54,56 This peak also has a lower frequency than the spectrum at 0.2 V due to the electrochemical Stark effect. Upon returning to 0.2 V in the anodic scan, a final spectrum in green reveals that the peak has returned to a similar frequency as the original cathodic peak, however, the intensity has increased slightly.

It is not possible to relate the potential-dependent intensity change to surface coverage without quantitatively accounting for dipole-dipole coupling as well as $\chi^{(3)}$ contributions. However, here we note that CO observed in the blue spectrum at +0.2 V prior to the onset of CO_2 reduction is the result of preliminary CV cycling, and a control experiment showing results for an electrode at a similar potential before any CV cycling shows that no CO is observed (see supporting information section 10). Additionally, the green spectrum, which is measured at the same potential following CO₂ reduction shows increased intensity, which cannot be solely the result of potential-dependent intensity changes. Both observations strongly suggest that the CO detected here is at least partly a result of the catalytic conversion of CO₂ to CO. However, relating these intensity changes to the potential dependent surface coverage would require a careful consideration of potential dependent $\chi^{(3)}$ contributions as well as the effects of dipole-dipole coupling. We anticipate that the ability to detect species at low coverage under relevant conditions of applied potential and faradaic current will facilitate further investigation of these phenomena, which are necessary to correlate potential-dependent frequency and intensity shifts to the actual molecular structure of these complex interfaces.

Many catalytic reactions, including CO₂ reduction, are sensitive to the surface morphology of the catalyst. This indicates that the nanostructured surface of the Au electrode that enables VSFG signal enhancement may also influence the resulting catalytic activity, which would represent a limitation of the current technique. To investigate this further, we measured the gas phase products produced during electrochemical CO₂ reduction on an identical Au electrode at -1.1 V vs Ag/AgCl and find that the faradaic efficiency is $38.1\pm1\%$ to CO and $64\pm1\%$ to H₂. This is in close agreement with previous studies on planar polycrystalline electrodes, ⁵⁷ indicating that the electrode surface structure is not significantly influencing the catalytic performance in the present case.

The ability to directly detect active species on elec-

trode surfaces is a long-standing challenge in electrocatalysis. Several studies have succeeded at observing transient CO on a Au surface from in-situ CO_2 reduction using Surface Enhanced Infrared Reflection-Absorption Spectroscopy (SEIRAS) 52,54 and Surface Enhanced Raman Spectroscopy (SERS), 56 and these studies reveal a complex potential dependent CO coverage, which is not yet fully understood. Even in these cases, detection often requires accumulation of CO at applied negative potentials prior to spectral measurement or the use of additives to increase the local concentration of CO near the electrode surface. The method reported here compliments these existing spectroelectrochemical methods by providing a sensitive and versatile technique for measuring surface intermediates under relevant electrocatalytic conditions.

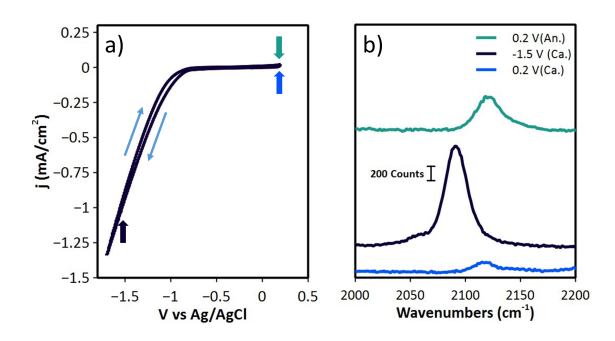


Figure 6. a) A cyclic voltammogram taken at 50 mV/s in the VSFG Cell. Thin arrows indicate the scan direction. The thicker colored arrows are color coordinated to the spectra in panel b and indicate the potential at which the spectra in panel b were taken. b) VSFG spectra of atop CO taken below and above the onset potential for $\rm CO_2$ reduction (Ca.- Cathodic Scan, An.- Anodic Scan). Spectra were recorded in 60 seconds using a step potential sequence.

4. Conclusions

In this work we have presented a method to probe species at the Au/electrolyte interface using off-angle momentummatched, plasmon-resonant VSFG spectroscopy. method has detection limits < 1% of a monolayer and can access the Au/electrolyte interface during active electrocatalysis. By enabling high sensitivity across a broad infrared spectral range at relevant applied potentials and high catalytic current densities, this technique overcomes a number of obstacles that have limited the application of VSFG for the study of electrochemical interfaces. To demonstrate the utility of this technique, we also report in-situ measurements of CO formed during active CO₂ reduction on Au and show that this is one of a very few techniques capable of measuring the low surface concentration of adsorbed CO under conditions of active catalytic turnover. We anticipate that this technique will improve molecular level understanding of electrochemical reactions by enabling direct detection of surface intermediates and electrolyte structure under relevant catalytic conditions.

Author Information

*Corresponding Author: baker.2364@osu.edu
The authors declare no competing financial interest.

Acknowledgements

This work was supported by National Science Foundation

under under NSF award number 1665280. XPS was performed at the OSU Surface Analysis Laboratory. Film deposition was performed at the OSU Nanosystems Laboratory. Electron microscopy was performed at the OSU Center for Electron Microscopy and Analysis (CEMAS). We thank the OSU College of Arts and Sciences machine shops for their help in fabrication of the VSFG system and electrochemical cell. We also thank Dr. Zachary Schultz for helpful discussions regarding plasmon resonances.

Supporting Information

The supporting material contains details of the 1. Experimental details of the electrochemical VSFG cell 2. VSFG spectra at various polarization combinations 3. SPR coupling mechanisms 4. Out of plane offset 5. Fitting a VSFG spectrum of dodecanethiol on gold 6. Calculations of three layer Fresnel factors 7. Importance of a nanostructured Au/CaF₂ interface 8. Extinction spectra of gold thin films as a function of film thickness 9. Determination of 4-mercaptobenzonitrile surface coverage using a competitive isotherm and 10. SFG spectra without preliminary CV cycling 11. Products of CO_2 reduction 12. Quadratic scaling of VSFG signal with surface concentration.

References

- (1) Liu, W.-T.; Shen, Y. R. In situ sum-frequency vibrational spectroscopy of electrochemical interfaces with surface plasmon resonance. Proc. Natl. Acad. Sci. U. S. A. 2014, 111, 1293-1297.
- Gardner, A. M.; Saeed, K. H.; Cowan, A. J. Vibrational sumfrequency generation spectroscopy of electrode surfaces: studying the mechanisms of sustainable fuel generation and utilisation. *Phys. Chem. Chem. Phys.* **2019**, *21*, 12067–12086.
- Tong, Y.; Lapointe, F.; Thämer, M.; Wolf, M.; Campen, R. K. Hydrophobic water probed experimentally at the gold electrode/aqueous interface. Angew. Chem., Int. Ed. 2017, 56, 4211-4214
- (4) Clark, M. L.; Ge, A.; Videla, P. E.; Rudshteyn, B.; Miller, C. J.; Song, J.; Batista, V. S.; Lian, T.; Kubiak, C. P. CO₂ reduction catalysts on gold electrode surfaces influenced by large electric fields. J. Am. Chem. Soc. 2018, 140, 17643–17655. Garcia Rey, N.; Dlott, D. D. Structural transition in an ionic
- liquid controls ${\rm CO_2}$ electrochemical reduction. J. Phys. Chem. C 2015, 119, 20892–20899. Sorenson, S. A.; Patrow, J. G.; Dawlaty, J. M. Solvation reaction
- field at the interface measured by vibrational sum frequency generation spectroscopy. J. Am. Chem. Soc. **2017**, 139, 2369–
- Hunt, J.; Guyot-Sionnest, P.; Shen, Y. Observation of CH stretch vibrations of monolayers of molecules optical sumfrequency generation. *Chem. Phys. Lett.* **1987**, *133*, 189–192.
- Lambert, A. G.; Davies, P. B.; Neivandt, D. J. Implementing the theory of sum frequency generation vibrational spectroscopy: a
- tutorial review. Appl. Spectrosc. Rev. 2005, 40, 103–145. Lagutchev, A.; Lozano, A.; Mukherjee, P.; Hambir, S. A.; Dlott, D. D. Compact broadband vibrational sum-frequency generation spectrometer with nonresonant suppression. Spectrochim. Acta, Part A 2010, 75, 1289–1296.
 Williams, C. T.; Yang, Y.; Bain, C. D. Total internal reflection
- sum-frequency spectroscopy: A strategy for studying molecular adsorption on metal surfaces. Langmuir 2000, 16, 2343–2350.
 Shi, H.; Cai, Z.; Patrow, J.; Zhao, B.; Wang, Y.; Wang, Y.; Benderskii, A.; Dawlaty, J.; Cronin, S. B. Monitoring Local Electric Fields at Electrode Surfaces Using Surface Enhanced Raman Scattering-Based Stark-Shift Spectroscopy during Hydrogen Evolution Reactions. ACS Appl. Mater. Interfaces 2018, 10. 33678–33683.
- (12) Thirumoorthi, M.; Thomas Joseph Prakash, J. Structure, optical and electrical properties of indium tin oxide ultra thin films prepared by jet nebulizer spray pyrolysis technique. J. Asian Ceram. Soc. **2016**, 4, 124–132.
- (13) Baldelli, S.; Markovic, N.; Ross, P.; Shen, Y.-R.; Somorjai, G. Sum frequency generation of CO on (111) and polycrystalline platinum electrode surfaces: evidence for SFG invisible surface
- CO. *J. Phys. Chem. B* **1999**, *103*, 8920–8925. Verreault, D.; Kurz, V.; Howell, C.; Koelsch, P. Sample cells for probing solid/liquid interfaces with broadband sum-frequencygeneration spectroscopy. Rev. Sci. Instrum. 2010, 81, 063111. Rey, N. G.; Dlott, D. D. Studies of electrochemical interfaces
- by broadband sum frequency generation. J. Electroanal. Chem. **2017**, 800, 114–125.

- (16) Patrow, J. G.: Sorenson, S. A.: Dawlaty, J. M. Direct spectroscopic measurement of interfacial electric fields near an electrode under polarizing or current-carrying conditions. J. Phys. Chem. C **2017**, *121*, 11585–11592.
- Löbau, J.; Wolfrum, K. Sum-frequency spectroscopy in total internal reflection geometry: signal enhancement and access to molecular properties. *J. Opt. Soc. Am. B* **1997**, *14*, 2505–2512. Nishi, N.; Hobara, D.; Yamamoto, M.; KAKIUCHI, T. Total-
- internal-reflection broad-bandwidth sum frequency generation spectroscopy of hexadecanethiol adsorbed on thin gold film de-
- posited on CaF₂. Analytical sciences **2003**, 19, 887–890. Tourillon, G.; Dreesen, L.; Volcke, C.; Sartenaer, Y.; Thiry, P. A.; Peremans, A. Total internal reflection sumfrequency generation spectroscopy and dense gold nanoparticles monolayer: a route for probing adsorbed molecules. Nanotechnology 2007, 18, 415301.
- Backus, E. H.; Garcia-Araez, N.; Bonn, M.; Bakker, H. J. On the role of Fresnel factors in sum-frequency generation spectroscopy of metal-water and metal-oxide-water interfaces. J.
- Phys. Chem. C 2012, 116, 23351–23361.
 Ye, S.; Nihonyanagi, S.; Fujishima, K.; Uosaki, K. Conformational Order of Octadecanethiol (ODT) Monolayer at Gold/Solution Interface: Internal Reflection Sum Frequency Generation (SFG) Study. Stud. Surf. Sci. Catal. 2001, 132,
- Humbert, C.; Noblet, T.; Dalstein, L.; Busson, B.; Barbillon, G. Sum-Frequency Generation Spectroscopy of Plasmonic Nanoma-
- terials: A Review. *Materials* **2019**, *12*, 836. Nihonyanagi, S.; Ye, S.; Uosaki, K.; Dreesen, L.; Humbert, C.; Thiry, P.; Peremans, A. Potential-dependent structure of the interfacial water on the gold electrode. Surf. Sci. 2004, 573,
- (24) Ekgasit, S.; Thammacharoen, C.; Knoll, W. Surface plasmon
- resonance spectroscopy based on evanescent field treatment. Anal. Chem. 2004, 76, 561–568.

 Akhade, S. A.; Luo, W.; Nie, X.; Bernstein, N. J.; Asthagiri, A.; Janik, M. J. Poisoning effect of adsorbed CO during CO₂ electroreduction on late transition metals. Phys. Chem. Chem. Phys. **2014**, 16, 20429–20435.
- Ringe, S.; Morales-Guio, C. G.; Chen, L. D.; Fields, M.; Jaramillo, T. F.; Hahn, C.; Chan, K. Double layer charging driven carbon dioxide adsorption limits the rate of electrochemical carbon dioxide reduction on Gold. *Nat. Commun* **2019**,
- Biswas, S.; Wallentine, S.; Bandaranayake, S.; Baker, L. R. Controlling polaron formation at hematite surfaces by molecular functionalization probed by XUV reflection-absorption spectroscopy. J. Chem. Phys. **2019**, 151, 104701.
 Raether, H. Surface plasmons on smooth and rough surfaces
- and on gratings; Springer, 1988; pp 4–39.

 (29) Hinman, S. S.; McKeating, K. S.; Cheng, Q. Surface plasmon
- resonance: material and interface design for universal accessi-
- bility. Anal. Chem. 2018, 90, 19-39.
 (30) Zayats, A. V.; Smolyaninov, I. I.; Maradudin, A. A. Nano-optics of surface plasmon polaritons. Phys. Rep. 2005, 408, 131-314.
 (31) Prabowo, B. A.; Purwidyantri, A.; Liu, K.-C. Surface plasmon
- resonance optical sensor: A review on light source technology. Biosensors 2018, 8, 80.
- Yang, J.; Sun, Q.; Ueno, K.; Shi, X.; Oshikiri, T.; Misawa, H.; Gong, Q. Manipulation of the dephasing time by strong coupling between localized and propagating surface plasmon modes. Nat. Commun. 2018, 9, 1–8.
- Chu, Y.; Crozier, K. B. Experimental study of the interaction between localized and propagating surface plasmons. Optics letters 2009, 34, 244-246.
- Lagutchev, A.; Hambir, S. A.; Dlott, D. D. Nonresonant background suppression in broadband vibrational sum-frequency generation spectroscopy. J. Phys. Chem. C 2007, 111, 13645
- Curtis, A. D.; Reynolds, S. B.; Calchera, A. R.; Patterson, J. E. Understanding the role of nonresonant sum-frequency generation from polystyrene thin films. J. Phys. Chem. Lett. 2010, 1, 2435 - 2439
- (36) Liu, M.; Pang, Y.; Zhang, B.; De Luna, P.; Voznyy, O.; Xu, J.; Zheng, X.; Dinh, C. T.; Fan, F.; Cao, C. et al. Enhanced electrocatalytic CO $_2$ reduction via field-induced reagent concentration. Nature 2016, 537, 382.
- Albert, G.; Maccarini, M.; Himmelhaus, M. Morphology of Thin Films of Gold Grown on CaF_2 (100) and (111). arXiv **2006**,
- Malinskỳ, P.; Slepička, P.; Hnatowicz, V.; Švorčík, V. Early stages of growth of gold layers sputter deposited on glass and silicon substrates. Nanoscale Res. Lett. 2012, 7, 241.
 Habteyes, T. G.; Dhuey, S.; Wood, E.; Gargas, D.; Cabrini, S.;
- Schuck, P. J.; Alivisatos, A. P.; Leone, S. R. Metallic adhesion layer induced plasmon damping and molecular linker as a nondamping alternative. ACS nano 2012, 6, 5702-5709.
- Chow, C.-M.; Bain, J. A. Effect of Thin Cr and Cu Adhesion Layers on Surface Plasmon Resonance at Au/SiO₂ Interfaces. Nanoscale Res. Lett. 2015, 52, 1-4.
- Mekhalif, Z.; Riga, J.; Pireaux, J.-J.; Delhalle, J. Self-assembled monolayers of n-dodecanethiol on electrochemically modified
- polycrystalline nickel surfaces. Langmuir 1997, 13, 2285–2290. Willets, K. A.; Van Duyne, R. P. Localized surface plasmon resonance spectroscopy and sensing. Annu. Rev. Phys. Chem.

- **2007**, 58, 267–297.
- Haes, A. J.; Van Duyne, R. P. A unified view of propagating and localized surface plasmon resonance biosensors. Anal. Bioanal. Chem. 2004, 379, 920-930.
- Yonzon, C.; Van Duyne, R. P. Localized and propagating surface plasmon resonance sensors: A study using carbohydrate binding protein. MRS Online Proc. Libr. 2005, 876.

 (45) Hammond, J. L.; Bhalla, N.; Rafiee, S. D.; Estrela, P. Localized
- surface plasmon resonance as a biosensing platform for develop-
- ing countries. Biosensors 2014, 4, 172–188. Sarkar, S.; Patrow, J. G.; Voegtle, M. J.; Pennathur, A. K.; Dawlaty, J. M. Electrodes as polarizing functional groups: Correlation between Hammett parameters and electrochemical polarization. J. Phys. Chem. C 2019, 123, 4926–4937.

 (47) Leverette, C. L.; Dluhy, R. A. Vibrational characterization
- of a planar-supported model bilayer system utilizing surface-enhanced Raman scattering (SERS) and infrared reflection absorption spectroscopy (IRRAS). Colloids Surf., A 2004, 243,
- 157–167.
 (48) Verger, F.; Pain, T.; Nazabal, V.; Boussard-Plédel, C.; Bureau, B.; Colas, F.; Rinnert, E.; Boukerma, K.; Compere, C.; Guilloux-Viry, M. et al. Surface enhanced infrared absorption (SEIRA) spectroscopy using gold nanoparticles on As₂S₃ glass. Sens. Actuators, B **2012**, 175, 142–148. (49) Kraack, J. P.; Kaech, A.; Hamm, P. Surface enhancement in
- ultrafast 2D ATR IR spectroscopy at the metal-liquid interface. J. Phys. Chem. C 2016, 120, 3350–3359.
- (50) Kraack, J. P.; Sévery, L.; Tilley, S. D.; Hamm, P. Plasmonic
- substrates do not promote vibrational energy transfer at solid—liquid interfaces. J. Phys. Chem. Lett. 2018, 9, 49–56.

 Dunwell, M.; Yang, X.; Setzler, B. P.; Anibal, J.; Yan, Y.; Xu, B. Examination of near-electrode concentration gradients and kinetic impacts on the electrochemical reduction of CO surface-enhanced infrared spectroscopy. ACS Catal. 2018, 8, 3999 - 4008.
- Wuttig, A.; Yaguchi, M.; Motobayashi, K.; Osawa, M.; Surendranath, Y. Inhibited proton transfer enhances Au-catalyzed CO₂-to-fuels selectivity. Proc. Natl. Acad. Sci. U. S. A. 2016, 113, E4585-E4593.
- (53) Raschke, M. B.; Shen, Y. R. Nonlinear optical spectroscopy of solid interfaces. Curr. Opin. Solid State Mater. Sci. 2004, 8, 343 - 352.
- (54) Dunwell, M.; Lu, Q.; Heyes, J. M.; Rosen, J.; Chen, J. G.; Yan, Y.; Jiao, F.; Xu, B. The central role of bicarbonate in the electrochemical reduction of carbon dioxide on gold. J. Am.
- Chem. Soc. **2017**, 139, 3774–3783. (55) Akhade, S. A.; Luo, W.; Nie, X.; Asthagiri, A.; Janik, M. J. Theoretical insight on reactivity trends in CO 2 electroreduction across transition metals. Catal. Sci. Technol. 2016, 6, 1042-
- (56) Oberst, J. L.; Kenis, P. J.; Gewirth, A. A., et al. Insight into the electrochemical reduction of ${\rm CO}_2$ on gold via surface-enhanced Raman spectroscopy and N-containing additives. J. Solid State Electrochem. 2016, 20, 1149–1154.
- Zhang, B. A.; Ozel, T.; Elias, J. S.; Costentin, C.; Nocera, D. G. Interplay of Homogeneous Reactions, Mass Transport, and Kinetics in Determining Selectivity of the Reduction of ${\rm CO}_2$ on Gold Electrodes. ACS Cent. Sci. **2019**,

Table of Contents Figure

